LLNL-JRNL-685720

LAWRENCE LIVERMORE NATIONAL LABORATORY

High Quantum Efficiency Photocathode Simulation for the Investigation of Novel Structured Designs

A. G. MacPhee, S. R. Nagel, P. M. Bell, D. K. Bradley, O. L. Landen, Y. P. Opachich, P. W. Ross, E. Huffman, J. Koch, T. J. Hilsabeck

March 11, 2016

High Quantum Efficiency Photocathode Simulation for the Investigation of Novel Structured Designs

High Quantum Efficiency Photocathode Simulation for the Investigation of Novel Structured Designs[a)]

Y. P. Opachich[1,b)], P. W. Ross[1], A. G. MacPhee[3], T. J. Hilsabeck[2], S. R. Nagel[3], E. Huffman[1], P. M. Bell[3], D. K. Bradley[3], J. Koch[1], O.L. Landen[3]

[1]*National Security Technologies, Livermore, CA 94550*

[2]*General Atomics, San Diego, CA 92121*

[3]*Lawrence Livermore National Laboratory, Livermore, CA 94551*

(Presented XXXXX; received XXXXX; accepted XXXXX; published online XXXXX)

(Dates appearing above are provided by the Editorial Office)

A computer model in CST Studio Suite has been developed to evaluate several novel geometrically enhanced photocathode designs. This work was aimed at identifying a structure that would increase the total electron yield by a factor of two or greater in the 1-30 keV range. The modeling software was used to simulate the electric field and generate particle tracking for several potential structures. The final photocathode structure has been tailored to meet a set of detector performance requirements, namely a spatial resolution of <40 um and a temporal spread of < 1 ps. This poster presents the details of the geometrically enhanced photocathode model and resulting static field and electron emission characteristics.

I. OVERVIEW

X-ray detectors, such as time dilation cameras and streak cameras are widely used in many applications ranging from laser driven plasma imaging to radiography and diffraction measurements. Recent advances in radiography have extended the imaging range well above 10 keV, and there is a significant need for an efficient photocathode in the in the spectral energy range from 1-30 keV. There have been a limited number of studies using structured photocathodes[1, 2], however up to date no reliable photocathode has been produced.

Detector efficiency and performance in the hard X-ray range is largely limited by the total quantum electron yield (TEY) and secondary electron kinetic energy distribution[3-6]. Most X-ray detectors operate at normal incidence, i.e. X-ray photons are at a 90º incidence angle to the photocathode, and suffer a loss in quantum efficiency at energies greater than 5 keV. Improvements in yield of up to 20 times [7], have been shown to occur in grazing incidence geometry, due to a larger path length of the x-ray photons which better matches the secondary electron escape depth within the photocathode material [8-12].

This work describes the details and results of a simulation used to identify a set of potential photocathode designs that leverage the grazing incidence geometry yield improvements, through the introduction of pillars or cavities to the photocathode substrate surface. The final structure consisted of a substrate with recessed cones of variable diameter and depth and showed a total yield improvement of ~2 times, without any significant compromise in spatial or temporal resolution.

II. THEORY AND COMPUTER SIMULATION DETAILS

The X-ray yield increase seen at grazing incidence has been verified experimentally[7], and a model has been developed by Fraser et. al, which accurately predicts the increase in total electron yield (TEY) as a function of angle of incidence and photon energy for the majority of commonly used photocathodes[9].

Assuming that the measured TEY consists mostly of secondary electrons[13], and that the fluorescent decay of the photoelectron is negligible [8], it can be shown that for a X-ray of energy E_x incident onto a photocathode of thickness T at an angle α, the secondary photocurrent, $(\chi_c)_s$ is given by [9]:

$$(\chi_c)_s = [1 - R(\alpha)] f P_s(0) E_x \varepsilon^{-1} (1+\beta)^{-1} Y(T)$$

Where $\beta = (\mu \operatorname{cosec} \alpha' L_s)^{-1}$, $R(\alpha)$ is the Fresnel reflectivity coefficient and α' is the angle of refraction of the X-ray beam. $P_s(0)$ is the secondary electron escape probability, ε is the energy needed to promote and electron above the valence band and escape into vacuum, μ is the linear absorption coefficient, f is the fraction of X-ray energy available for generation of secondary electrons, L_s is the secondary electron escape length, and $Y(T)$ is the relative yield-versus-thickness function $Y(T) = 1 - \exp[-(\mu \operatorname{cosec} \alpha' + L_s^{-1})T]$. This simplified equation was used to determine the expected yield as a function of angle and X-ray energy for CsI and Au. The resulting TEY is plotted as a function of energy in Figure 1. A structure wall angle of 10 -15 degrees was chosen based on these results.

A computer simulation, in CST Studio Suite [14] was used to identify a structure that would satisfy several X-ray detector performance requirements: Spatial resolution of 40 microns or better and a temporal resolution of 1-10 ps. The resulting field gradient, electron trajectories, energies, velocities and angular distributions were simulated using this technology. The model was also used to predict the performance of two photocathode materials, CsI and Au by choosing the appropriate secondary electron energy and angular distributions [13]. The simulations were performed for a cathode to mesh gap of 1mm with electric field ranging from 3125 V/mm to 10000 V/mm. All results presented in the paper had a 3125 V/mm field, which is used in the Dilation X-ray Imager (DIXI)[15, 16]. A resulting electric field simulation of the recessed cone geometry is shown in Figure 2.

[a)]Contributed (or Invited) paper published as part of the Proceedings of the 20th Topical Conference on High-Temperature Plasma Diagnostics, Atlanta, Georgia, June, 2014.

[b)]Author to whom correspondence should be addressed: email@none.edu

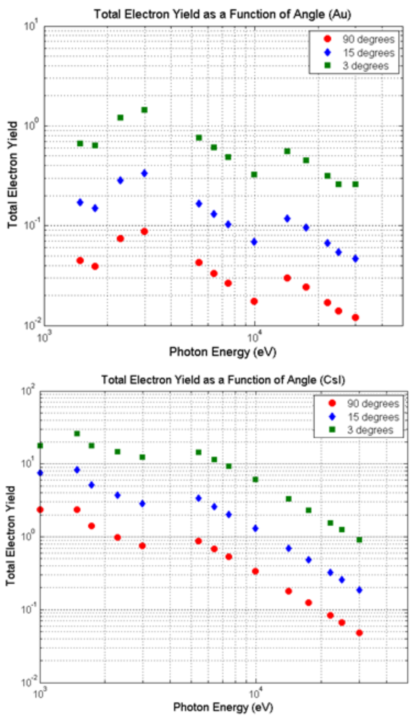

FIG. 1. Total Electron Yield as a function of angle of incidence and X-ray energy for the 1-30 keV energy range for Au and CsI photocathode materials.

III. RESULTS AND DISCUSSION

The detector performance requirements used for the qualification of the photocathode design presented in this work are derived from instruments which utilize micro-channel plates as imagers or have complex imaging systems. Hence, any contribution to the spatial and temporal resolution from the secondary electron distribution in the acceleration gap region (cathode to mesh anode) of these cameras has been assumed to be minimal and ignored. Geometrically enhanced photocathodes do introduce a sizeable spatial and temporal spread to the electron distribution, which depend on the structure depth and diameter. CST was used to fully simulate the temporal, spatial and angular spread of electrons that are generated at the structured photocathode surface and leave the acceleration region and compared to the nominal detector requirements.

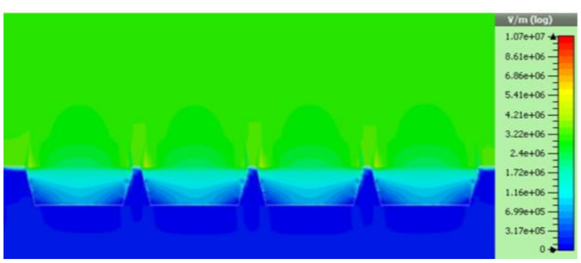

FIG. 2. CST suite field gradient simulation for recessed cone geometry for structures that are 6 µm in diameter and 3 µm deep.

The spatial resolution of the recessed cone photocathode is limited by the trajectory of electrons generated at the cone walls. See Figure 3. These electrons follow parabolic paths with a final resolution element radius that depends on the photocathode material, along with the diameter and angle of the structure. A small degradation in spatial resolution was seen when comparing the performance of CsI to that of Au, due to a difference in the initial kinetic energy of the electrons generated at the photocathode surface. The smallest radius and depth was set by the strength of the field gradient within the cavity, this corresponded to a diameter of 4 um and depth of 2 um and corresponded to a spatial resolution element of ~40 um at the output of the acceleration gap region, see Figure 4. Smaller spatial resolution is possible by choosing an appropriate diameter to depth ratio of the cavity.

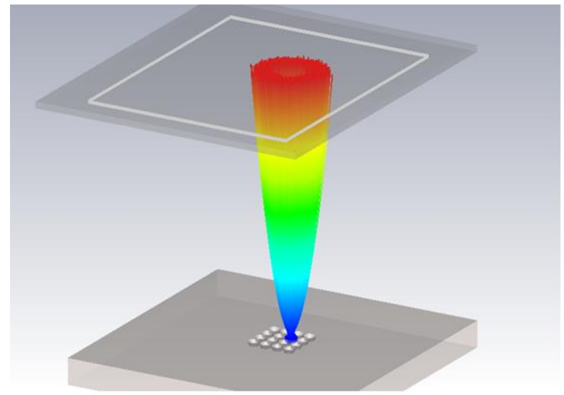

FIG. 3. The resulting spatial resolution element as set by the recessed cone structure parameters.

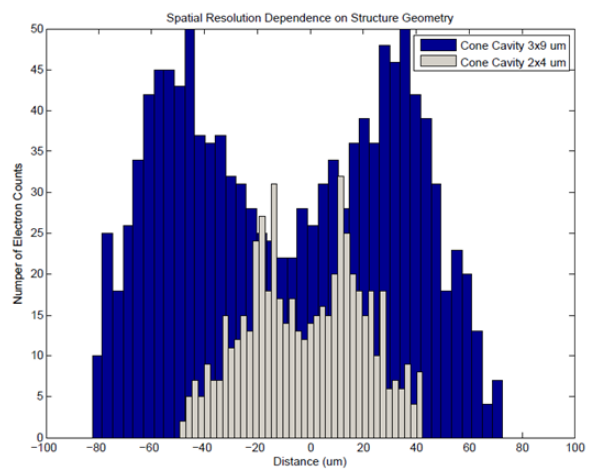

FIG. 4. The dependence of the spatial resolution on the outer diameter of the recessed cavity structure.

The temporal resolution of the recessed cone photocathode showed a dependence on the cavity depth, and the angle of the cavity walls. The largest contributor to the temporal spread comes from electrons generated at the cavity bottom. A temporal difference of 980 fs was calculated for a structure with a depth of 3 um, and a wall angle of 15 degrees. Increasing the cavity depth, reduced the field gradient within the cavity and had the effect of increasing the temporal spread in the emitted electron distribution. The current photocathode design is within the temporal resolution of many x-ray detectors, with a ~1 ps record resolution.

The recessed cone geometry showed a small increase in the angular divergence of the electron distribution at the exit plane of the acceleration region when compared to a planar photocathode.

A 5 mrad angular spread was seen for a planar photocathode, in comparison to a 25 mrad for an electrons emitted from the structured photocathode. This small effect should not degrade the spatial resolution of most detectors, however should be simulated for a full detector performance study.

The total electron yield emitted from the structured photocathode is the sum of the yield from the planar photocathode regions and from the angled surfaces which provide the yield enhancement. The predicted enhanced yield contribution is calculated for a projected surface area onto the top planar surface. The sum total for the structured photocathode resolution element is then compared to the total electron yield from a standard planar photocathode. The calculated yield increase for a set of structured photocathode parameters is listed in Table 1. The total yield increase for our design is on the order of 2 times, which is largely driven by the spatial and temporal resolution requirements of a given X-ray detector. It is conceivable that an increase as large as four times, however this will degrade the temporal performance of the photocathode. A recessed pyramid structure, which has a slightly better yield performance, has also been considered. The final prototype design will be set by ease of etching of our substrate material.

TABLE 1. List of photocathode structure types, parameters and the expected total electron yield at 14 keV.

Geometry	Incidence Angle	Diameter μm	Height μm	Au TEY	CsI TEY
Cone	15	6	3	1.76	1.77
Pyramid	15	6	3	1.85	1.85
Cone	15	4	2	1.66	1.67
Pyramid	15	4	2	1.74	1.74
Cone	10	6	3	1.88	1.87
Pyramid	10	6	3	2.12	2.11
Cone	10	4	2	1.77	1.76
Pyramid	10	4	2	1.97	1.97

IV. CONCLUSIONS

A computer model has been developed for the purpose of identifying a geometrically enhanced photocathode structure that withstands a high field gradient, has a spatial resolution of ~40 um or better and temporal resolution that is smaller than ~1 ps. The structure utilized the near grazing incidence effect to increase the total electron yield from Au and CsI photocathodes in the 1-30 keV range. Recessed cone geometry was identified as a potential photocathode design, and the CST model has proven to be a flexible and useful tool for future photocathode design. The results of this study will be used to build and test a prototype, and the topic of future publications.

IV. REFERENCES

1. C. Halvorson, Rev. Sci. Instrum. **81** (10), 10E309 (2010).
2. G. Potdevin, Universite Joseph Fourier, 2008.
3. J. Feng, H. J. Shin, J. R. Nasiatka, W. Wan, A. T. Young, G. Huang, A. Comin, J. Byrd and H. A. Padmore, Applied Physics Letters **91** (13), 134102-134102-134103 (2007).
4. J. Feng, W. Wan, J. Qiang, A. Bartelt, A. Comin, A. Scholl, J. Byrd, R. Falcone, G. Huang, A. MacPhee, J. Nasiatka, K. Opachich, D. Weinstein, T. Young and H. A. Padmore, 2005 (unpublished).
5. Y. P. Opachich, University of California at Davis, 2011.
6. Y. P. Opachich, D. H. Kalantar, A. G. MacPhee, J. P. Holder, J. R. Kimbrough, P. M. Bell, D. K. Bradley, B. Hatch, G. Brienza-Larsen, C. Brown, C. G. Brown, D. Browning, M. Charest, E. L. Dewald, M. Griffin, B. Guidry, M. J. Haugh, D. G. Hicks, D. Homoelle, J. J. Lee, A. J. Mackinnon, A. Mead, N. Palmer, B. H. Perfect, J. S. Ross, C. Silbernagel and O. Landen, Review of Scientific Instruments **83** (12), 125105 (2012).
7. D. P. Lowney, P. A. Heimann, H. A. Padmore, E. M. Gullikson, A. G. MacPhee and R. W. Falcone, Review of Scientific Instruments **75** (10), 3131-3137 (2004).
8. G. W. Fraser, Nuclear Instruments and Methods in Physics Research **206** (1-2), 265-279 (1983).
9. G. W. Fraser, Nuclear Instruments and Methods in Physics Research **206** (1-2), 251-263 (1983).
10. B. L. Henke, Physical Review A (General Physics) **6** (1), 94-104 (1972).
11. B. L. Henke, J. Liesegang and S. D. Smith, Physical Review B **19** (6), 3004-3021 (1979).
12. B. L. Henke, J. A. Smith and D. T. Attwood, Journal of Applied Physics **48** (5), 1852-1866 (1977).
13. B. L. Henke, J. P. Knauer and K. Premaratne, Journal of Applied Physics **52** (3), 1509-1520 (1981).
14. CST, (2014).
15. S. R. Nagel, T. J. Hilsabeck, P. M. Bell, D. K. Bradley, M. J. Ayers, M. A. Barrios, B. Felker, R. F. Smith, G. W. Collins, O. S. Jones, J. D. Kilkenny, T. Chung, K. Piston, K. S. Raman, B. Sammuli, J. D. Hares and A. K. L. Dymoke-Bradshaw, Review of Scientific Instruments **83** (10E116) (2012).
16. T. J. Hilsabeck, J. D. Hares, J. D. Kilkenny, P. M. Bell, A. K. L. Dymoke-Bradshaw, J. A. Koch, P. M. Celliers, D. K. Bradley, T. McCarville, M. Pivovaroff, R. Soufli and R. Bionta, Review of Scientific Instruments **81** (10E317) (2010).

Prepared by LLNL under Contract DE-AC52-07NA27344.